frontiers | Frontiers in Materials

TYPE Original Research
PUBLISHED 15 November 2024
DOI 10.3389/fmats.2024.1501604

OPEN ACCESS

EDITED BY
Afshin Marani,
University of Toronto, Canada

REVIEWED BY
Pavlo Maruschak,
Ternopil Ivan Pului National Technical University, Ukraine
Armin Jamali,
Queen's University Belfast, United Kingdom

*CORRESPONDENCE
Ninghui Sun,
1172593203@qq.com
Yinghao Liang,
yinghao@163.com

RECEIVED 25 September 2024
ACCEPTED 30 October 2024
PUBLISHED 15 November 2024

CITATION
Wei W, He Q, Pang S, Ji S, Cheng Y, Sun N and Liang Y (2024) Enhancing crack self-healing properties of low-carbon LC3 cement using microbial induced calcite precipitation technique.
Front. Mater. 11:1501604.
doi: 10.3389/fmats.2024.1501604

Enhancing crack self-healing properties of low-carbon LC3 cement using microbial induced calcite precipitation technique

Wenzhu Wei[1], Qinglong He[2], Sen Pang[1], Shengjie Ji[1], Yiluo Cheng[3], Ninghui Sun[4]* and Yinghao Liang[4]*

[1]Beijing Building Research Institute Corporation Ltd. of The China State Construction Engineering Corporation, Beijing, China, [2]Institute of Computing Technology, Chinese Academy of Sciences, Beijing, China, [3]Dalian Maritime University, Dalian City, Liaoning Province, China, [4]School of Civil and Transportation Engineering, Hebei University of Technology, Tianjin, China

Limestone Calcined Clay Cement (LC3) is a promising low-carbon alternative to traditional cement, but its reduced clinker content limits its self-healing ability for microcracks, affecting durability. This study explores the application of Microbial Induced Calcite Precipitation (MICP) technique to enhance the crack self-healing capacity of LC3-based materials. *Bacillus pasteurii* was utilized to induce calcium carbonate precipitation to improve the crack self-healing capacity of LC3, thereby addressing its limited durability due to reduced clinker content. Experimental tests focused on optimizing the growth conditions for *B. pasteurii*, evaluating the compressive strength, capillary water absorption, and crack self-healing rates of the modified LC3 material. Results showed that under optimal conditions (pH of 9, inoculation volume of 10%, incubation temperature of 30°C, and shaking speed of 150 rpm), the bacterial strain exhibited maximum metabolic activity. The Microbe-LC3 mortar demonstrated a self-healing rate of up to 97% for cracks narrower than 100 μm, significantly higher than unmodified LC3. Additionally, the compressive strength of Microbe-LC3 was enhanced by approximately 15% compared to standard LC3 mortar after 28 days. The capillary water absorption was reduced, indicating improved durability due to the microbial-induced calcium carbonate filling the pores. This study confirms that MICP technology is a viable approach to significantly enhance the performance of LC3, contributing to the development of more durable and sustainable cementitious materials for construction applications.

KEYWORDS

limestone calcined clay cement, microbial induced calcite precipitation, *Bacillus pasteurii*, crack self-healing, compressive strength, low-carbon cementitious materials

1 Introduction

In recent years, with the advent of green and sustainable development principles, the issues of high carbon emissions and energy consumption in the construction industry have increasingly come under scrutiny (Zhao et al., 2023; Wang et al., 2024a). Cement, as one of the most widely used construction materials in civil engineering,

has consistently maintained a high level of demand and production (Barbhuiya et al., 2024). Currently, global cement production exceeds four billion tons annually, with approximately 0.83 tons of carbon dioxide emitted for every ton of cement clinker produced (Zhang et al., 2024a). Statistics indicate that CO_2 emissions from traditional cement production account for 5%–8% of the total global carbon emissions (Pillai et al., 2019). As CO_2 is a major greenhouse gas contributing to the greenhouse effect, its significant emissions directly exacerbate global warming, leading to extreme weather events, rising sea levels, and reductions in biodiversity (Scheiner, 2024; Hu et al., 2024). Therefore, reducing carbon emissions and energy consumption in the cement production process remains a key focus in the field of construction materials (Guo Y. et al., 2024).

Currently, the use of supplementary cementitious materials (SCMs) has become a key strategy for addressing the high carbon emissions and high energy consumption associated with cement production (Skibsted and Snellings, 2019; Pacheco Torgal et al., 2012; Benjamin et al., 2024). Among these, fly ash and slag are widely used SCMs and have been extensively studied by researchers (Lee et al., 2019; Wu et al., 2024; Liu et al., 2022). However, as the application range of SCMs expands and the pressure to conserve energy and reduce emissions increases, fly ash and slag are no longer sufficient to meet production demands. In contrast, the extensive availability of clay and limestone makes them advantageous SCMs for producing low-carbon cement (Matschei et al., 2007; Emmanuel et al., 2016). Calcined clay and limestone, as SCMs, offer significant development potential compared to other materials (Fode et al., 2023; Mañosa et al., 2024; Li et al., 2024). Limestone Calcined Clay Cement (LC3), which is composed of limestone, calcined clay, and clinker, provides a higher clinker substitution rate compared to ordinary Portland cement. The use of LC3 can reduce CO_2 emissions by 30%–40% (Zunino and Scrivener, 2022; Al-Fakih et al., 2023). Additionally, the calcined clay and limestone in LC3, used as SCMs, enhance the hydration and mineralization processes, thereby ensuring the cement's excellent performance (Shao and Cao, 2024; Scrivener et al., 2018). With its low cost, low energy consumption, reduced carbon emissions, and good service performance, LC3 is a promising choice.

It is important to note that, compared to traditional cement-based materials, LC3 based materials have a lower clinker content and reduced amounts of calcium hydroxide hydration products, which limits their mineralization capacity. Consequently, LC3 exhibits a poorer self-healing ability for microcracks, which adversely impacts its durability. Furthermore, concrete structures inevitably develop microcracks and cracks due to various external forces and environmental factors (Wang et al., 2019). The formation of microcracks not only diminishes the mechanical performance and durability of cement-based materials but also increases maintenance and repair costs over time (Zhang Y. S. et al., 2024; Khaliq and Ehsan, 2016; Li and Li, 2019).

Currently, traditional methods for repairing cracks in cement-based materials primarily rely on manual intervention and routine maintenance. Common repair techniques include epoxy resin injection, grouting, and electrophoretic deposition (Leng et al., 2024; Chen et al., 2024; Chang et al., 2009). Liu F. et al. (2024) investigated the crack resistance of a composite structure using magnesium phosphate cement mortar as an overlay for Portland cement concrete and found that the magnesium phosphate cement mortar overlay could prevent cracks from propagating through the concrete. Chu et al. (2020) studied the impact of electrophoretic deposition on the microstructure of concrete and discovered that electrophoretic deposition has a repair effect on concrete cracks, with the deposited material positively influencing the overall density of the concrete. Gujar et al. (2020), by studying the interfacial fracture energy between cement paste and epoxy coatings, proposed the use of high molecular weight methyl methacrylate to repair concrete cracks. However, traditional repair methods are passive, require significant labor and resources, and often lack durability, while also causing substantial environmental pollution (Lu et al., 2023; Althoey et al., 2023). Therefore, there is a need to seek new, efficient solutions.

Based on the principles of green development, microbiologically induced calcite precipitation (MICP) technology, which integrates microbiology and geochemistry, has rapidly advanced both domestically and internationally in recent years. MICP is an emerging biomineralization technique (Wang et al., 2023; Fouladi et al., 2023).The primary principle of this technology is that microorganisms produce carbonate ions through their metabolic processes. These carbonate ions then react with calcium ions in the environment to quickly form calcite crystals, which have binding properties (Prajapati et al., 2023; Wang et al., 2024b). When applied to self-healing concrete, MICP technology can use the calcium carbonate precipitated by microorganisms to fill cracks, thereby achieving self-repair. Compared to traditional concrete crack repair methods, the microbiological mineralization repair technique not only enhances the self-healing ability of concrete and improves material durability but also reduces maintenance costs and lessens environmental impact (Du et al., 2020).

This study aims to enhance the crack self-healing capacity of LC3 based materials by applying MICP technology, thereby improving the material's durability and service life and addressing the deficiencies arising from clinker substitution. This study, based on experimental fundamentals, conducted tests on microbial activity, crack self-healing rate, compressive strength of cement mortar, capillary water absorption of cement mortar, and SEM-EDS (scanning electron microscopy and energy-dispersive X-ray spectroscopy). The goal is to elucidate the self-healing mechanism of cracks in Microbe -LC3 materials and scientifically validate the feasibility of this type of cement, providing theoretical guidance for practical engineering applications.

2 Materials and methods

2.1 Raw materials

The main materials used in the microbial experiments include *Bacillus pasteurii* (North Bio Company, strain ATCC 11859; Gram-positive; rod-shaped cells, 2–3 μm in length; spherical spores, 0.5–1.5 μm in length), beef extract, urea, peptone, calcium nitrate, and deionized water. All reagents used in the experiments are sourced from the China National Pharmaceutical Group Chemical Reagents Platform. Before utilizing the microorganisms, they need to be cultured in advance. The culture medium components include beef extract (6 g/L), soybean peptone (10 g/L), urea (30 g/L), and

TABLE 1 Particle size analysis of calcined kaolin.

	D_{10}	D_{25}	D_{50}	D_{75}	D_{90}
Particle size (μm)	0.61	1.14	2.11	5.68	9.13

deionized water. The prepared medium is then aliquoted into wide-mouth triangle flasks and subjected to sterilization in a high-pressure steam autoclave at 121°C for 20 min. After sterilization, under sterile conditions in an ultra-clean table, the medium in the triangle flasks is inoculated with *Bacillus* pasteurii. Finally, the inoculated medium is incubated in a shaking incubator at 30°C, with a rotation speed of 150 rpm, for 48 h.

The primary materials used in the cement-based material experiments include Ordinary Portland Cement (Grade 52.5), limestone powder, calcined clay, sand and fiber (PVA). The Ordinary Portland Cement (OPC) is supplied by Shandong Kang Jing New Materials Technology Co., Ltd. The limestone powder is a fine, super-white heavy calcium carbonate produced by Tianjin Yan Dong Mineral Products Co., Ltd. The calcined clay, sourced from Yichang, Hubei, has its particle size distribution analyzed using a laser particle size analyzer (JL—1155), with results provided in Table 1. Chemical composition analysis of the cement, limestone, and calcined clay is conducted using X-ray Fluorescence, with the chemical compositions listed in Table 2.

2.2 Experimental design

The experiment initially focused on determining the optimal growth conditions for *B. pasteurii* by varying pH, temperature, shaking speed, and inoculation volume. Based on these optimal conditions, the microbial mineralization technique was employed, using *B. pasteurii* as the mineralizing agent to modify LC3. The effectiveness of microbial mineralization in enhancing the self-healing properties of low-carbon LC3 materials was investigated through compressive strength tests, capillary water absorption tests, micro-crack self-healing rate tests, and microstructural characterization using SEM-EDS. Three cement mortar mix ratios were designed for the experiment: M1 represents the OPC mortar group; M2 represents the LC3 mortar group; and M3 represents the Microbe-LC3 mortar group. The composition ratios for each experimental group are detailed in Table 3. It should be noted that the quantities of bacterial solution, calcium nitrate, and urea have been optimized for effective microbial-induced calcite precipitation, resulting in enhanced performance of the modified LC3 materials. However, further experiments could explore varying these amounts to achieve additional improvements in self-healing, durability, or mechanical properties.

2.3 Sample preparation

The experiment utilized a planetary mixer to prepare the specimens. Initially, the solid materials were dry mixed for 3 min. Subsequently, water and bacterial solution were gradually and uniformly added, and mixing continued for an additional 3 min. The prepared cement mortar was then poured into molds and vibrated on a vibration table for approximately 2 min to remove any air bubbles. Three types of test specimens were prepared: cylindrical specimens with a diameter of 5 cm and a height of 1.5 cm for crack observation; cylindrical specimens with a diameter of 10 cm and a height of 5 cm for water absorption tests; and cubic specimens measuring 50 cm × 50 cm × 50 cm for compressive strength testing. After casting, the specimens were cured at room temperature (25°C) and relative humidity of 40%–50%. To prevent excessive moisture evaporation, the specimens were covered with plastic film. After 24 h of curing, the specimens were demolded and then maintained at room temperature until performance testing.

2.4 Test methods

2.4.1 Microbial concentration detection

The experiment employs the optical density (OD) turbidity method to assess microbial growth by measuring the amount of transmitted light as an indirect indicator of bacterial concentration. The fundamental principle is based on the selective absorption of light by substances. A solution with light-absorbing properties will reduce the energy of monochromatic light passing through it. As the concentration of the solution increases, the light energy absorbed increases accordingly. Therefore, when light passes through a bacterial suspension, it is absorbed and scattered, causing changes in the amount of transmitted light in relation to the concentration of the bacterial suspension. As the bacterial count increases, the absorbance rises and the transmittance decreases. Thus, a spectrophotometer is used to measure the bacterial concentration, with the wavelength set to 600 nm, and the measurements are expressed as OD600.

2.4.2 Uniaxial compressive strength test

The uniaxial compressive strength tests are conducted using a uniaxial compressive testing machine (YAWS-2500J, China), in accordance with the GB/T 50,081–2002 standard (China, 2002). A total of 27 cubic specimens (50 cm × 50 cm × 50 cm) are used for the compressive strength tests, with nine specimens in each of the groups M1, M2, and M3. There are three specimens designated for compressive strength testing at the ages of 7, 14, and 28 days, with the average results representing the unconfined compressive strength at the corresponding ages.

2.4.3 Capillary water absorption test

The capillary water absorption tests are performed on cylindrical specimens with a diameter of 10 cm and a height of 5 cm at 28 days), in accordance with the ASTM C1585 standard (Int, 2013). All specimens are dried in an oven at 50°C. The sides of the specimens were sealed with waterproof tape to ensure that water penetrated only from the bottom, achieving unidirectional contact. The top was sealed with plastic wrap and secured with a rubber band to prevent moisture evaporation. The water level was maintained 3–5 mm above the bottom surface of the specimens. Two wooden sticks were placed under the specimens to increase the contact area between the bottom of the specimens and the water. The experimental setup is illustrated in Figure 1. At fixed time intervals (1 min, 5 min, 10 min, 20 min, 30 min, 1 h, 2 h, 3 h, 4 h, 5 h, 6 h), the specimens were removed from the water, and the surface moisture was wiped off before measuring the water absorption. A total of nine cylindrical specimens (10 cm in diameter and 5 cm in height)

TABLE 2 Oxide composition of cement, limestone, calcined clay (wt%).

Oxide	CaO	SiO_2	Al_2O_3	Fe_2O_3	MgO	Na_2O	K_2O	SO_3	TiO_2	$CaCO_3$	LOI
Cement	69.58	16.42	4.77	3.10	1.72	0.20	0.60	2.64	0.47	—	0.29
calcined clay	0.35	50.33	45.91	0.66	0.36	0.10	0.27	0.01	—	—	0.11
Limestone	—	0.02	0.012	0.02	0.07	—	—	—	—	98.75	2.90

were used for the capillary water absorption tests, with three specimens allocated to each of the M1, M2, and M3 groups. The water absorption rate for each group was calculated as the average of the results from the three specimens. The formulas 1, 2 for calculating water absorption are as follows:

$$I = \frac{m_t}{a \times d} \tag{1}$$

$$S = \frac{I}{\sqrt{t}} \tag{2}$$

where: m_t represents the mass change of the specimen at time t, in g. a, denotes the area of contact between the bottom of the specimen and the water, in mm^2. d indicates the density of water, in g/mm^3. S is the water absorption coefficient.

2.4.4 Crack self-healing rate test

To simulate the cracking phenomenon of cement mortar under working conditions, a small bench vise was used to artificially create cracks in cylindrical specimens with a diameter of 5 cm and a height of 1.5 cm. Given the fracture characteristics of the experimental materials, a compressive force perpendicular to the axis of the specimen was applied to induce failure and generate cracks (Figure 2). The cracks were observed using a digital microscope, and the images were processed into binary slices using Origin software to distinguish the cracks. The width of the cracks on the specimen surfaces before and after self-healing was recorded using HiView software. A total of 18 cylindrical specimens (diameter: 5 cm, height:1.5 cm) are used for the crack self-healing experiments, with six specimens in each of the groups M1, M2, and M3. Each specimen has eight observation areas for crack self-healing. Regulations concerning repair indicators are referenced according to the BSEN-1504 standard (Strompinis et al., 2014). The formula 3 for calculating the crack self-healing rate is:

$$\mathcal{R} = \left[\frac{(W_0 - W_t)}{W_0}\right] \times 100\% \tag{3}$$

where: W_0 is the width of the cracks before self-healing. W_t is the width of the cracks after self-healing.

2.4.5 SEM-EDS

The scanning electron microscope (SEM) equipped with energy-dispersive X-ray spectroscopy (EDS) (SU3800, GUI 3D) was utilized to observe the microstructural morphology and elemental composition of the self-healing material filling the cracks after 28 days. The SEM was operated at an accelerating voltage of 20 kV and magnifications ranging from 500 to 1,500 times. Prior to SEM-EDS analysis, the specimens were coated with gold using a Q150T sputter coater. The gold coating process involved two sputtering cycles within 60 s, with a current of 20 mA.

3 Results

3.1 Optimization of microbial culture conditions

The growth of *B. pasteurii* is influenced by various factors. Through optimizing the cultivation conditions of this strain, a deeper understanding of its physiological characteristics, adaptation mechanisms, growth curve, and metabolic pathways can be achieved. This optimization aims to enhance the strain's activity and application effectiveness, thereby maximizing resource utilization efficiency and reducing economic costs.

The pH regulates the physiological characteristics, metabolic processes, and activity of the strain (Gat et al., 2017). Figure 3A shows the impact of pH on the growth of *B. pasteurii*. It can be observed that, within the alkaline pH range of 7–12, the OD600 value of *B. pasteurii* initially increases and then decreases as pH increases. This indicates that the growth rate of *B. pasteurii* initially increases and then declines. Specifically, the growth of *B. pasteurii* is optimal at a pH of 9, where bacterial metabolic activity is most vigorous and the growth rate is the highest. However, at a pH of 12, the growth of *B. pasteurii* is significantly inhibited. While *B. pasteurii* can grow in alkaline environments, extreme alkaline conditions may adversely affect its growth, including enzyme activity and cell membrane stability (Mobley et al., 1995). Additionally, studies have shown that both acidic and strongly alkaline conditions can disrupt the metabolism of *B. pasteurii* and its production of urease, potentially rendering the produced enzyme irreversibly inactive (Mobley et al., 1995; Ciurli et al., 1996).

Temperature is also a crucial factor affecting strain activity, stability, spore formation, and growth rate (Sun et al., 2019; Yi et al., 2021). Figure 3C illustrates the impact of temperature on the growth of *B. pasteurii*. The growth curve of the strain shows that as the incubation temperature increases from 25°C to 35°C, the OD600 value of *B. pasteurii* initially increases and then decreases. The OD600 value peaks at 30°C, indicate that this temperature is most suitable for the growth of *B. pasteurii*. The experimental results are consistent with previous studies, which shows that *B. pasteurii* exhibits optimal growth and metabolic activity around 30°C (Yi et al., 2021; Kim et al., 2018; Omoregie et al., 2017).

The inoculation amount of microorganisms in the culture medium is crucial, as both excessively high and low inoculation levels can affect microbial growth. Figure 3B illustrates the impact

10.3389/fmats.2024.1501604

TABLE 3 Composition ratio of cement mortar test block.

Group	Cement (g)	Limestone powder (g)	Calcined clay (g)	Sand (g)	Water (mL)	Urea (g)	Calcium nitrate (g)	Bacterial solution (mL)	W/B	PVA (g)
M1	850	0	0	1700	382.5	0	0	0	0.45	6
M2	595	85	170	1700	382.5	0	0	0	0.45	6
M3	595	85	170	1700	306	15	20	72.5	0.45	6

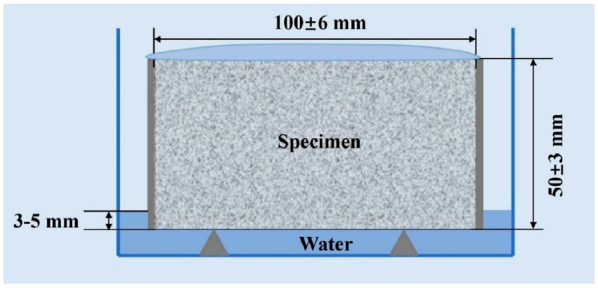

FIGURE 1
Water absorption experimental device diagram.

of inoculation amounts on the growth of *B. pasteurii*. When the inoculation volume is 5% of the total culture medium, compared to 10%, 15%, and 20%, the bacterial concentration and growth rate are significantly lower. A lower inoculation amount results in insufficient microbial colonies, leading to slower growth rates due to the reduced concentration of bacteria (Panikov, 2023). Conversely, a higher initial bacterial concentration can accelerate growth and reproduction. However, an excessively high inoculation amount may lead to resource competition, thereby inhibiting microbial growth (Guo L. et al., 2024). Considering the adverse effects of both extreme cases on *B. pasteurii* growth, an inoculation level of 10% is deemed appropriate.

For microbial growth in liquid culture media, mechanical shaking techniques can create a favorable environment for microorganisms, enhancing their growth and metabolic processes. Continuous shaking increases the surface area of contact between the culture medium and air, which is especially crucial for aerobic microorganisms, facilitating their faster and more complete growth. Additionally, shaking helps to evenly distribute nutrients and microorganisms in the culture medium, preventing issues such as cell sedimentation and nutrient unevenness that can occur in static cultures. Figure 3D illustrates the effect of shaking speed on the growth of *B. pasteurii*. In the figure, 1 mL and 1.5 mL refer to the volumes of *Bacillus* spores inoculated into the culture medium, while the corresponding rpm indicates the shaking speed of the medium in the shaker. As shown in Figure 3D, the optical density of the bacterial culture is highest at a shaking speed of 150 rpm, indicating that *B. pasteurii* exhibits optimal growth under this condition.

Through the optimization study of *B. pasteurii* cultivation conditions, it was found that the optimal growth environment for *B. pasteurii* is achieved when the pH of the culture medium is maintained at 9, the inoculation amount is 10%, the shaking speed in the incubator is set to 150 rpm, and the temperature is at 30°C. The growth curve of *B. pasteurii* under these conditions is shown in Figure 4.

3.2 Uniaxial compressive strength

Figure 5 presents the compressive strength of 50 mm × 50 mm × 50 mm cubic samples at curing ages of 7, 14, and 28 days. It is evident from the figure that the compressive strength of the OPC mortar samples (M1 group) is higher at 7, 14, and 28 days compared

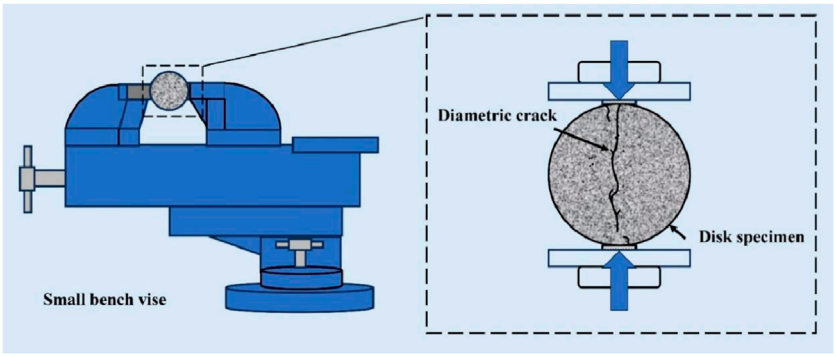

FIGURE 2
Schematic diagram of creating cracks.

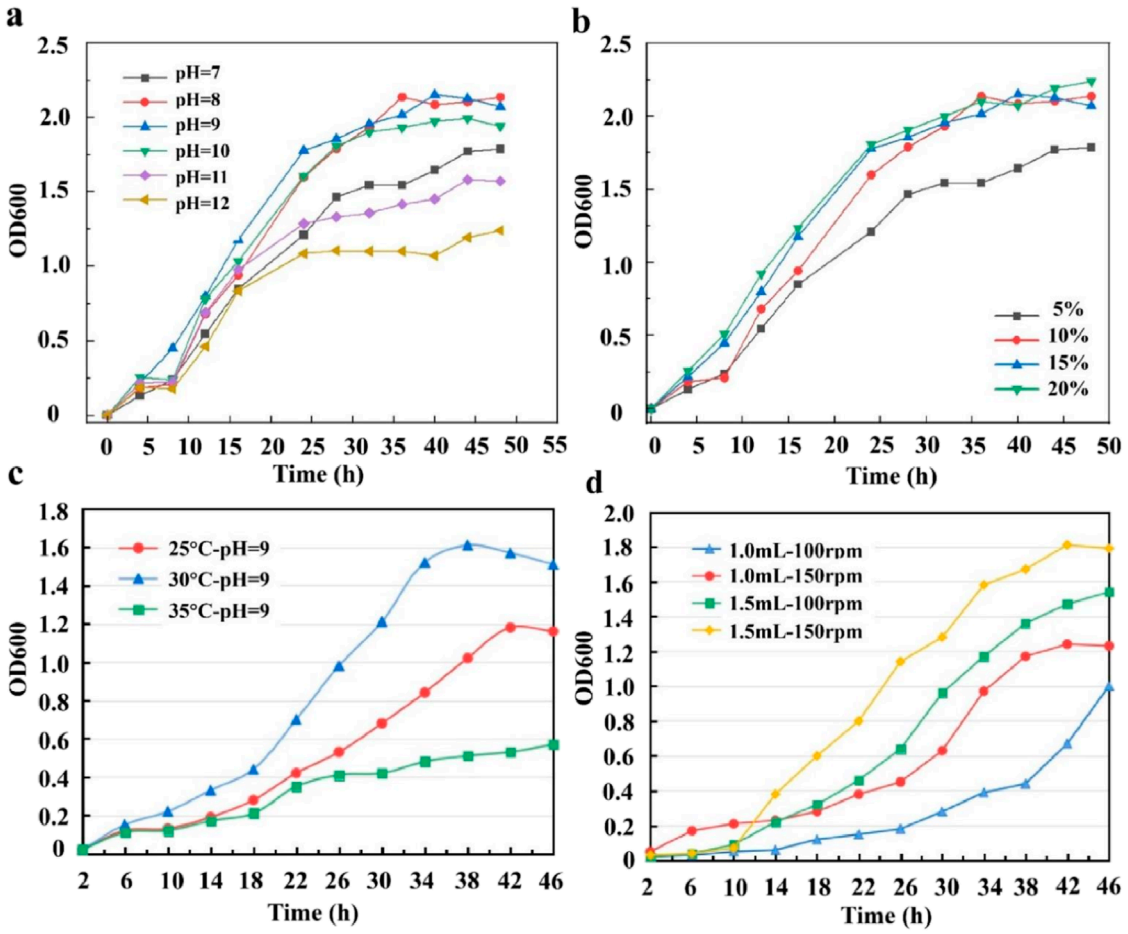

FIGURE 3
Growth curves of *Bacillus pasteurii* under different culture conditions. The growth curves of *Bacillus pasteurii* **(A)** at different pH values, **(B)** in different inoculated quantities, **(C)** under different temperature conditions, and **(D)** at different oscillating speeds.

to the LC3 mortar samples (M2 and M3 groups). The partial replacement of cement with calcined clay and limestone powder has led to a decrease in mechanical performance. Specifically, the compressive strength of the LC3 mortar samples decreased by approximately 20% compared to the OPC mortar samples. The decrease in compressive strength is primarily attributed to the partial replacement of ordinary cement with calcined clay and limestone in LC3. The addition of calcined clay has led to a significant refinement of the pore structure in the cementitious system (Tironi et al., 2014). Research indicates that the hydration

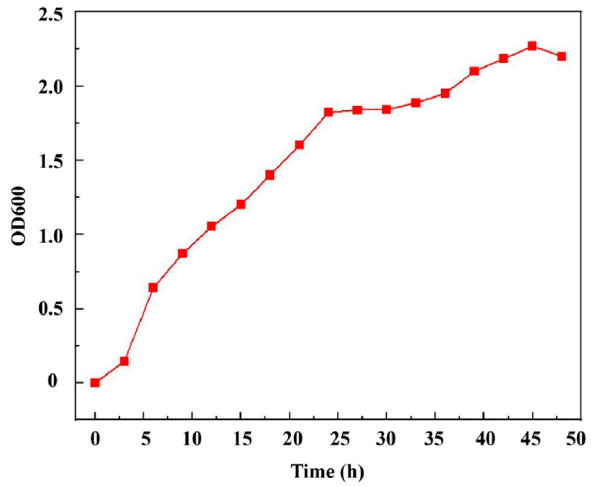

FIGURE 4
Growth curve of *Bacillus pasteurii* under optimal conditions.

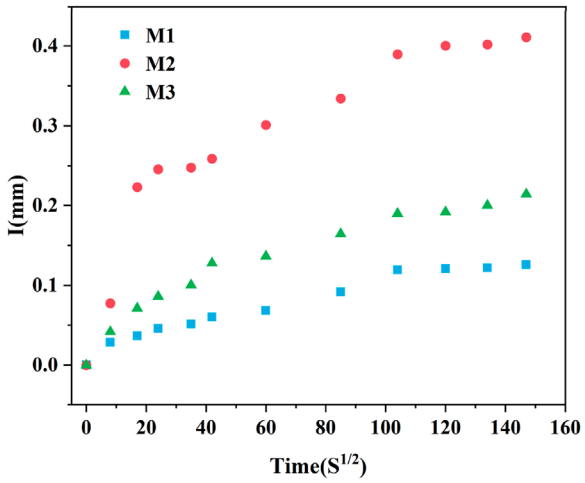

FIGURE 6
Water absorption regression curve.

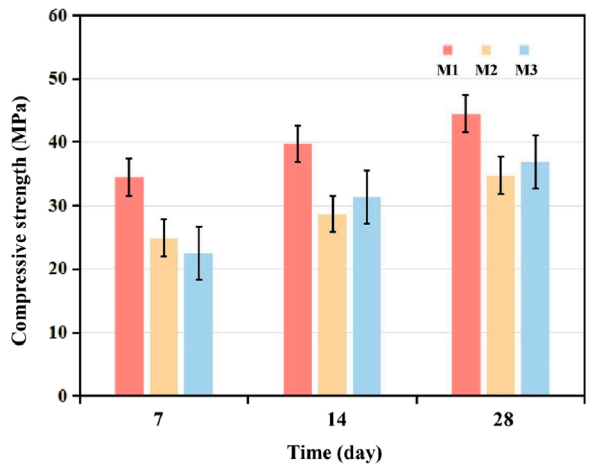

FIGURE 5
Compressive strength of cement mortar specimen.

rate of clinker is related to the internal pore structure of the material; refined pores are less conducive to the hydration reactions (Avet and Scrivener, 2018). Consequently, the refined pore structure slows down the hydration rate of the clinker, resulting in reduced long-term hydration of C_3S and C_2S, and a suppression of the formation of AFm phases, carbonate-aluminate phases, and other hydration products (Krishnan et al., 2019; Antoni et al., 2012). Additionally, among the two types of LC3 mortar specimens, the Microbe-LC3 mortar specimen in the M3 group showed improved compressive strength at both 14 and 28 days compared to the LC3 mortar specimen in the M2 group. This enhancement is primarily due to the positive effect of microbial incorporation on strength development. The calcium carbonate precipitation induced by *B. pasteurii* mineralization improves the internal pore structure, resulting in a denser and more cohesive matrix, thereby increasing the compressive strength (Mondal and Ghosh, 2023).

3.3 Capillary water absorption

Figure 6 shows the water absorption regression curves of cement mortar specimens at specific time intervals. From the figure, it is observed that the M1 group of OPC mortar specimens has the lowest water absorption rate, while the M2 group of LC3 mortar specimens exhibits significantly higher water absorption compared to both M1 and M3. The increased water absorption rate is likely due to the slower early hydration rate and incomplete hydration of LC3 mortar, which results in a less dense internal pore structure. Consequently, the higher capillary porosity in the LC3 mortar leads to a higher water absorption rate compared to OPC mortar.

Furthermore, the capillary water absorption rate of the M3 group (Microbe-LC3 mortar) is significantly lower than that of the M2 group (LC3 mortar). The presence of microorganisms in the M3 group introduces a dual-component coating system with capillary pore-blocking characteristics. First, microorganisms can deposit on the surface of the cement matrix and form a biofilm, which blocks a certain number of capillary pores. Additionally, microorganisms act as nucleation sites, leading to the formation of a carbonate coating under the MICP process. This dual-component coating system, consisting of microorganisms and carbonate deposits, plays a crucial role in reducing the material's water absorption rate by effectively blocking capillary pores (De Muynck et al., 2008; Tiano et al., 1999).

3.4 Crack self-healing rate

Figure 7 illustrates the surface crack self-healing results for specimens from the M1 group (OPC mortar). Figure 8 presents the surface crack self-healing observations for specimens from the M2 group (LC3 mortar). Figure 9 shows the surface crack self-healing results for specimens from the M3 group (Microbe-LC3 mortar). A comparison of the observed images of surface crack self-healing across the different groups reveals that the M2 group (LC3 mortar) exhibits the poorest self-healing performance. Compared to the other two groups, the width of the repaired cracks is significantly

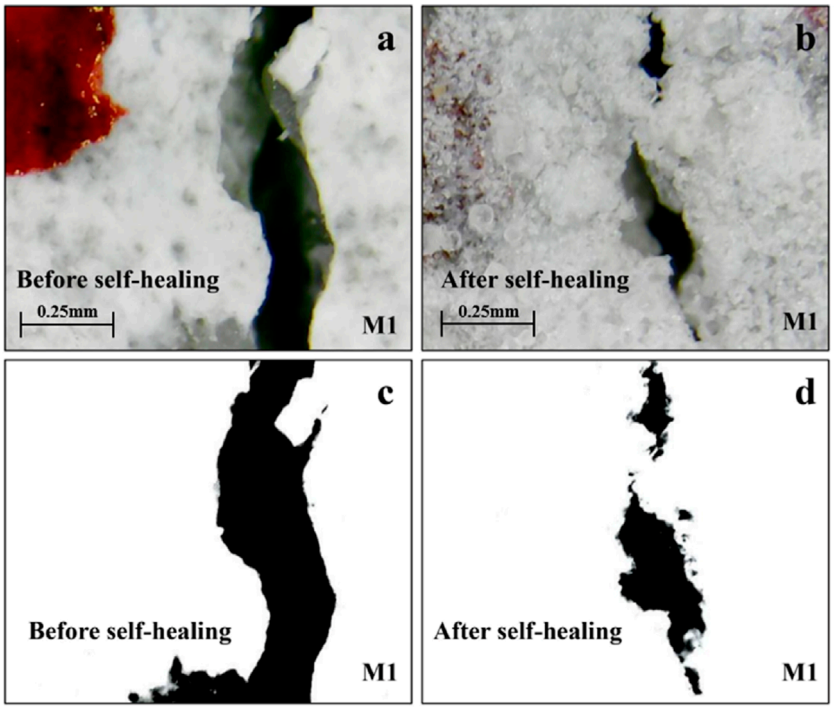

FIGURE 7
Comparison image of crack self-healing before and after 28 days of specimens in group M1. **(A)**, Before self-healing. **(B)**, After self-healing. **(C)**, Binary processing diagram corresponding to "a". **(D)**, Binary processing diagram corresponding to "b".

smaller, and the formation of crystalline deposits within the cracks is minimal. The M1 group (OPC mortar) shows somewhat better repair performance, although complete repair is not achieved, with larger areas remaining unfilled and gaps present. In contrast, the M3 group (Microbe-LC3 mortar) demonstrates nearly complete crack repair, with dense and fully covering crystalline deposits, showing the best results. For the crystalline deposits, SEM results (Figure 10) reveal that the deposits at cracks P1 and P2 in the M2 group appear as spherical aggregates. In comparison, the deposits at cracks P3 and P4 in the M3 group display a significantly different morphology. The particles are smaller and more densely connected. The differences in the morphology and distribution of $CaCO_3$ crystals are attributed to the presence of *B. pasteurii*. The MICP process enhances mineralization efficiency, leading to increased $CaCO_3$ production and a denser arrangement of the deposits. Additionally, the microorganisms themselves serve as nucleation sites, and factors such as microbial metabolic activity, cell surface structure, and biofilm formation influence the crystal morphology of the precipitates. During metabolism, microorganisms also produce organic substances that bind the mineral precipitates together, resulting in an irregular and dense distribution (Liu H. et al., 2024).

Additionally, as shown in Figure 10B, PVA fibers are covered by calcium carbonate crystals. This indicates that PVA fibers can promote the precipitation of calcium carbonate by providing preferred nucleation sites. The impact of PVA fibers on improving the precipitation of self-repair products in LC3 materials can be attributed to the unique molecular structure of their hydroxyl groups (Feng et al., 2019a). PVA fiber molecules interact with ions in the surrounding environment through intermolecular forces such as van der Waals forces, ionic bonds, and hydrogen bonds. This interaction aids in the aggregation and precipitation of calcium ions, thereby promoting the formation of calcium carbonate (Homma et al., 2009). Additionally, in aqueous solutions, hydroxyl groups can form hydrogen bonds with water molecules, enhancing their affinity for water. This strong interaction can increase the ionic concentration around the hydroxyl groups (Guan et al., 2017). Hydroxyl radicals can serve as nucleation centers, further promoting the binding of calcium ions and carbonate ions, and synergistically accelerating the repair of cracks in LC3 cement-based materials alongside microbial mineralization.

To further investigate the crack self-healing capabilities of the different cement mortar specimens, the self-healing performance was quantified by measuring the crack widths before and after the repair process. As shown in Figure 11, the self-healing rate of specimens in the M2 group is significantly lower than that of the other two groups. The M3 group exhibits the highest self-healing rate, achieving up to approximately 97% repair efficiency for cracks narrower than 100 μm, while for cracks with widths between 100 and 300 μm, the repair rate remains above 80%. Notably, the M3 group does not experience a significant decrease in repair efficiency as crack width increases, unlike the other two groups. The differences in crack self-healing capabilities between the M1 and M2 groups are likely due to the characteristics of LC3 compared to OPC. LC3 has a lower clinker content, which results in a reduced amount of $Ca(OH)_2$ produced during the hydration process. This lower concentration of $Ca(OH)_2$ limits the availability of calcium ions for mineralization

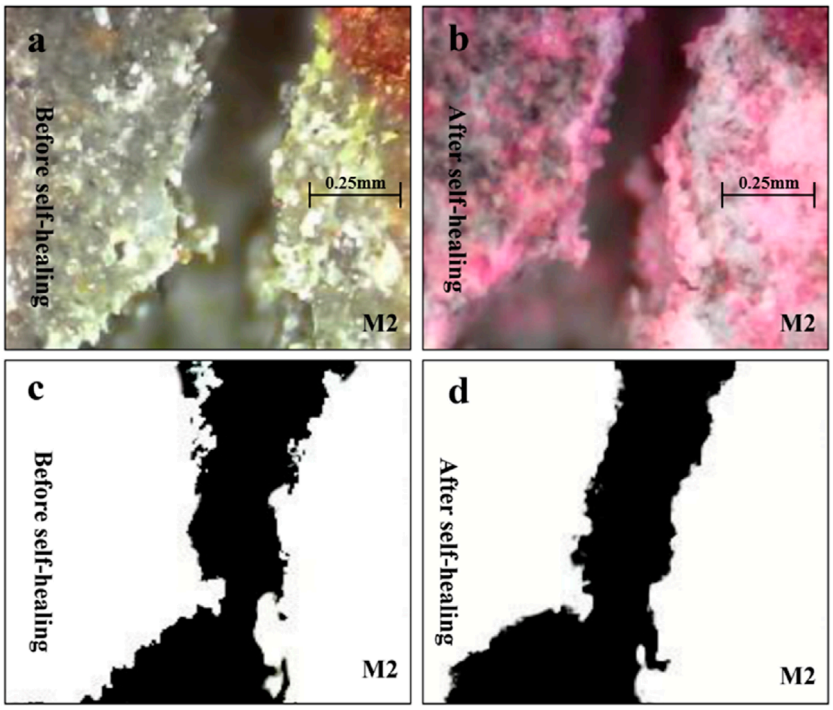

FIGURE 8
Comparison image of crack self-healing before and after 28 days of specimens in group M2. **(A)**, Before self-healing. **(B)**, After self-healing. **(C)**, Binary processing diagram corresponding to "a". **(D)**, Binary processing diagram corresponding to "b".

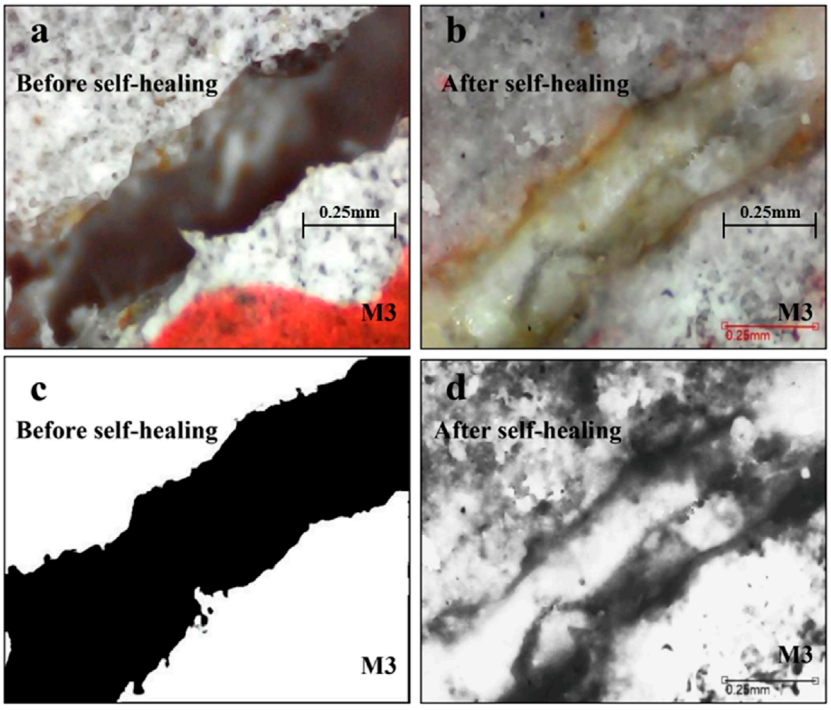

FIGURE 9
Comparison image of crack self-healing before and after 28 days of specimens in group M3. **(A)**, Before self-healing. **(B)**, After self-healing. **(C)**, Binary processing diagram corresponding to "a". **(D)**, Binary processing diagram corresponding to "b".

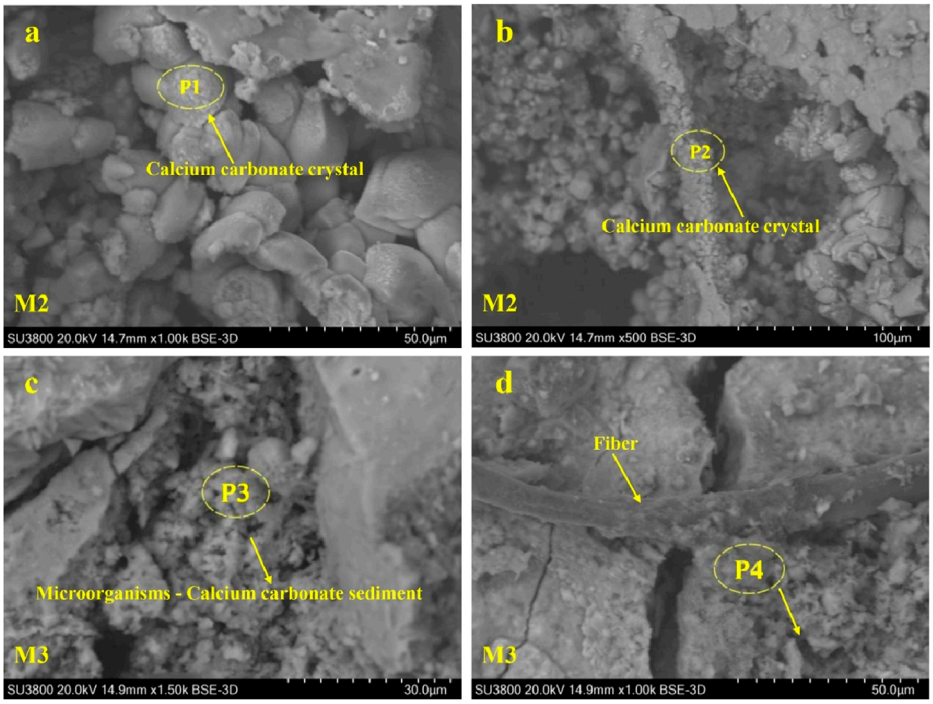

FIGURE 10
The microstructure of the crystal product at the crack of the specimen. **(A, B)**, Microstructure of the crystal product at the crack of M2 group specimen. **(C, D)**, Microstructure of the crystal product at the crack of M3 group specimen.

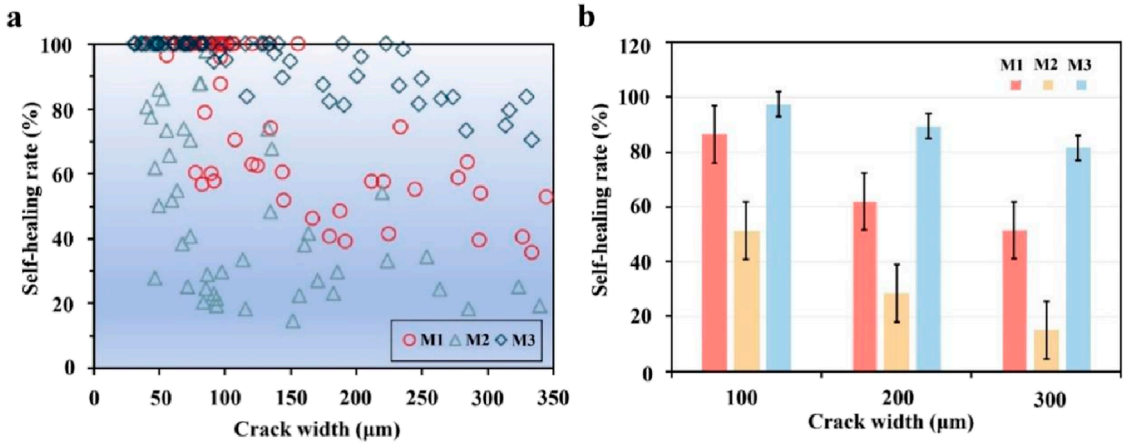

FIGURE 11
Effect of crack width on self-healing rate. **(A)**, Scatter plot of self-healing rate corresponding to crack width. **(B)**, Histogram of average self-healing rate corresponding to crack width.

and thus impairs the ability to repair cracks. Therefore, the self-healing capability of LC3 based materials is less than that of OPC based materials.

The superior crack self-healing ability of the M3 group, consisting of Microbe-LC3 mortar specimens, can be attributed to both inherent self-healing processes and the accelerated self-healing effects facilitated by microorganisms (De Muynck et al., 2008). Inherent self-healing primarily involves the reaction of CO_2 from the air, which dissolves in water to form unstable carbonic acid. In an alkaline environment provided by the cement matrix, carbonic acid readily decomposes into carbonate ions. These carbonate ions react with calcium ions released from the LC3 matrix, leading to the precipitation of $CaCO_3$ within the cracks and reducing their width. Compared to inherent self-healing, the accelerated self-healing facilitated by microorganisms plays a more crucial role. When urease-producing bacteria are incorporated into LC3 based

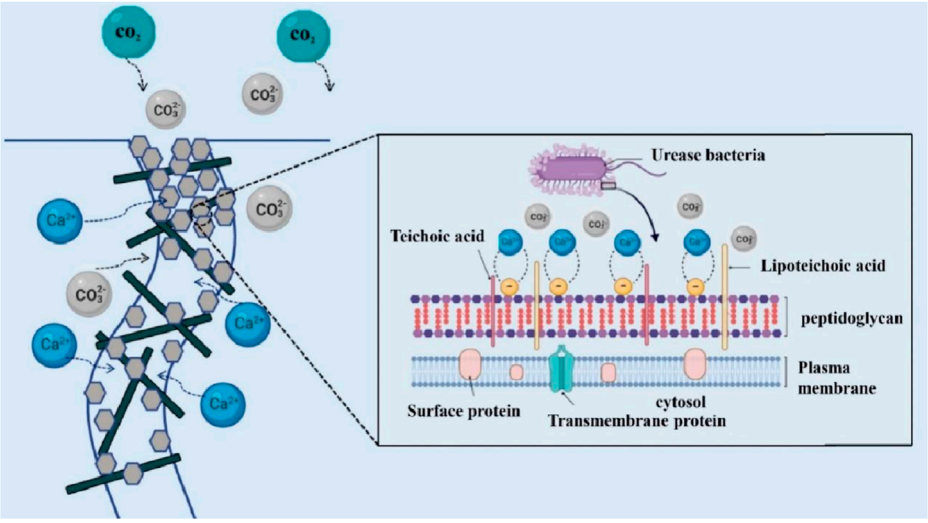

FIGURE 12
Mechanism of crack self-healing led by microbial mineralization.

materials, the lack of oxygen and moisture in the matrix initially causes the bacteria to enter a dormant state. Upon the formation of cracks, water and oxygen infiltrate, reactivating the bacterial spores near the cracks. The bacteria produce a significant amount of carbonate ions through the action of urease. The inclusion of external calcium sources during the mixing of Microbe-LC3 mortar enhances the dissolution of calcium ions, which further accelerates the precipitation of calcium carbonate, thus improving the efficiency of crack repair (Turner et al., 2023).

In Microbe-LC3 materials, the self-healing mechanism of cracks driven by MICP technology is influenced by several critical factors, including urease, dissolved calcium ions, and nucleation sites (Feng et al., 2019b). The primary role of microorganisms is to produce urease, which catalyzes the hydrolysis of urea to provide the carbonate ions necessary for calcium carbonate precipitation. Additionally, microorganisms serve as nucleation sites for the continuous and stable deposition of calcium carbonate (Wang et al., 2021; Zhang et al., 2024c). As illustrated in Figure 12, urease-producing bacteria are encased by multiple layers of peptidoglycan in their cell walls, where small particulate precipitates can be induced and retained (Liu H. et al., 2024; De Belie and De Muynck, 2008). Furthermore, the presence of fatty acids containing functional groups such as phosphate and carboxyl groups imparts a negative charge to the cell walls, facilitating the attraction and binding of metal cations (calcium ions) to the bacterial surface (Scott and Barnett, 2006; Castro-Alonso et al., 2019). The mechanism of MICP is related to formulas 4–7.

$$NH_2 - CO - NH_2 + H_2O \xrightarrow{urease} 2NH_3 + CO_2 \quad (4)$$

$$NH_3 + H_2O \leftrightarrow NH_4^+ + OH^- \quad (5)$$

$$CO_2 + OH^- \rightarrow HCO_3^- \quad (6)$$

$$Cell - Ca^{2+} + HCO_3^{2-} + OH^- \rightarrow Cell - CaCO_3 + H_2O \quad (7)$$

4 Discussion

The objective of this study was to enhance the durability and crack self-healing properties of low-carbon LC3 by utilizing MICP technology. Specifically, the aim was to address the durability challenges posed by LC3's reduced clinker content and limited microcrack healing capacity. The research involved optimizing the growth conditions for *B. pasteurii* and applying it to LC3 mortar to investigate its effects on compressive strength, capillary water absorption, and crack self-healing performance. These experiments were conducted to explore the potential of microbial mineralization to improve the overall mechanical and durability properties of LC3, providing a sustainable alternative to traditional cementitious materials.

The research results indicate that the application of microbial mineralization technology in cement-based materials effectively enhances the performance of LC3 mortar by promoting the precipitation of calcium carbonate. Firstly, the MICP technology significantly improves the self-healing capability of LC3 mortar, achieving a self-healing rate of up to 97% for cracks less than 100 μm in width. Secondly, after 28 days, the compressive strength of Microbe-LC3 mortar was found to be 15% higher than that of standard LC3 mortar. Additionally, the precipitation of calcium carbonate within the pore structure notably reduced the capillary water absorption, thereby improving the durability of the mortar. These findings demonstrate that the integration of microbial mineralization technology not only addresses the durability limitations of LC3 but also enhances its mechanical properties, positioning it as a promising sustainable building material.

The results of this study are of significant importance as they demonstrate the feasibility of using MICP technology to enhance the crack healing capability and durability of LC3 materials. The microbial-induced calcium carbonate precipitation plays a critical role in filling microcracks and capillary pores, thereby improving the structural integrity of LC3-based materials.

These findings are consistent with previous studies that highlight the benefits of microbial mineralization in improving material properties (Fouladi et al., 2023; Gebru et al., 2021; Kirkland et al., 2019). Similar improvements in mechanical strength and durability have been reported in studies involving the incorporation of microorganisms into cementitious materials (Zhang W. et al., 2024; Rathivarman et al., 2024; Mutitu et al., 2019). The main parameter used to evaluate the quality of concrete after self-healing was the crack self-healing rate, measured by the reduction in crack width before and after healing. The Microbe-LC3 mortar demonstrated a repair efficiency of up to 97% for cracks narrower than 100 μm, highlighting the effectiveness of MICP in enhancing crack closure and improving durability.

The mechanical properties of the repaired concrete (modulus of elasticity, creep, and shrinkage) will indeed differ from those of the original concrete due to the combined influence of the *Bacillus* pasteurii-induced calcite precipitation and the original crack morphology. The parameters of the repaired material will largely be governed by the nature and extent of crack healing, as well as the microstructure of the newly formed material and its interaction with the existing concrete matrix. This heterogeneity should be taken into account when assessing the long-term performance of self-healing concrete materials. In recent years, intellectualized and automated approaches for crack detection and analysis, such as the method proposed by Maruschak et al. (2016), have been increasingly utilized in materials science. These methods leverage advanced algorithms for crack binarization, allowing for more precise analysis of the crack front. These techniques offer significant improvements in the analysis of fatigue damage and automated detection, which could complement the binary image processing method employed in this study. Future research could explore the integration of such automated approaches to enhance the detection and analysis of cracks in cementitious materials.

The broader implications of these findings lie in the potential for widespread adoption of LC3 as a sustainable construction material. The successful application of MICP technology to enhance LC3's performance addresses critical concerns regarding its durability and mechanical properties, which could accelerate the material's acceptance in the industry. Furthermore, the environmental benefits of using a low-carbon material, combined with the reduced need for maintenance and repairs due to improved self-healing capabilities, present an attractive solution for addressing climate change in the construction sector.

While the study produced promising results, it is important to acknowledge certain limitations. The experiments were conducted under controlled laboratory conditions, which may not fully represent real-world construction environments. The long-term performance of Microbe-LC3 in varying environmental conditions, such as exposure to fluctuating temperatures and humidity, was not explored in this study. Additionally, the self-healing process was dependent on the availability of moisture to reactivate the microorganisms, which may limit its effectiveness in dry environments. These factors should be considered when interpreting the results and applying them in practice.

Future research should focus on addressing the limitations identified in this study. Investigating the long-term performance of Microbe-LC3 under different environmental conditions would provide a more comprehensive understanding of its durability in real-world applications. Additionally, exploring alternative microbial strains or modifying the MICP process could further enhance the efficiency of crack self-healing in LC3 materials. Research should also explore the potential for scaling up the technology for large-scale construction projects, ensuring that the benefits observed in laboratory settings can be replicated in practical applications.

5 Conclusion

This study successfully applied microbial-induced calcite precipitation (MICP) to improve the self-healing and mechanical properties of low-carbon LC3 cement. The key scientific contribution lies in demonstrating that MICP technology, utilizing *Bacillus* pasteurii, can effectively enhance the self-healing efficiency of LC3, achieving a crack closure rate of up to 97% for cracks narrower than 100 μm. Additionally, the modified LC3 showed a 15% improvement in compressive strength compared to unmodified LC3, highlighting the potential for enhancing both the durability and mechanical performance of low-clinker cementitious materials. The results address the challenge of reduced self-healing capacity in LC3 due to its lower clinker content, offering a novel, sustainable approach to improving the material's long-term performance. These findings provide a solid foundation for further research on optimizing MICP in other low-carbon cement systems, contributing to the development of more durable and environmentally friendly construction materials. To account for cases where healing occurs primarily within the crack but not at the surface, supplementary methods (such as micro-CT or ultrasonic techniques) should be used in the future work, and a layered or depth-specific approach can be applied to refine the self-healing rate evaluation.

Data availability statement

The original contributions presented in the study are included in the article/supplementary material, further inquiries can be directed to the corresponding authors.

Author contributions

WW: Conceptualization, Writing–review and editing. QH: Investigation, Writing–review and editing. SP: Data curation, Writing–review and editing. SJ: Methodology, Writing–review and editing. YC: Supervision, Writing–review and editing. NS: Writing–original draft, Writing–review and editing. YL: Writing–review and editing.

Funding

The author(s) declare that financial support was received for the research, authorship, and/or publication of this article. The authors

would like to acknowledge the support provided by Education Department of Hebei Province (grant number: CXY2024041).

Conflict of interest

Authors WW, SP, and SJ were employed by Beijing Building Research Institute Corporation Ltd. of The China State Construction Engineering Corporation.

The remaining authors declare that the research was conducted in the absence of any commercial or financial relationships that could be construed as a potential conflict of interest.

Generative AI statement

The author(s) declare that no Generative AI was used in the creation of this manuscript.

Publisher's note

All claims expressed in this article are solely those of the authors and do not necessarily represent those of their affiliated organizations, or those of the publisher, the editors and the reviewers. Any product that may be evaluated in this article, or claim that may be made by its manufacturer, is not guaranteed or endorsed by the publisher.

References

Al-Fakih, A., Al-Shugaa, M. A., Al-Osta, M. A., and Thomas, B. S. (2023). Mechanical, environmental, and economic performance of engineered cementitious composite incorporated limestone calcined clay cement: a review. *J. Build. Eng.* 79, 107901. doi:10.1016/j.jobe.2023.107901

Althoey, F., Zaid, O., Arbili, M. M., Martínez-García, R., Alhamami, A., Shah, H. A., et al. (2023). Physical, strength, durability and microstructural analysis of self-healing concrete: a systematic review. *Case Stud. Constr. Mater.* 18, e01730. doi:10.1016/j.cscm.2022.e01730

Antoni, M., Rossen, J., Martirena, F., and Scrivener, K. (2012). Cement substitution by a combination of metakaolin and limestone. *Cem. Concr. Res.* 42, 1579–1589. doi:10.1016/j.cemconres.2012.09.006

Avet, F., and Scrivener, K. (2018). Investigation of the calcined kaolinite content on the hydration of limestone calcined clay cement (LC3). *Cem. Concr. Res.* 107, 124–135. doi:10.1016/j.cemconres.2018.02.016

Barbhuiya, S., Bhusan Das, B., and Adak, D. (2024). Roadmap to a net-zero carbon cement sector: strategies, innovations and policy imperatives. *J. Environ. Manag.* 359, 121052. doi:10.1016/j.jenvman.2024.121052

Benjamin, B., Zachariah, S., Sudhakumar, J., and Suchithra, T. V. (2024). Harnessing construction biotechnology for sustainable upcycled cement composites: a meta-analytical review. *J. Build. Eng.* 86, 108973. doi:10.1016/j.jobe.2024.108973

Castro-Alonso, M. J., Montañez-Hernandez, L. E., Sanchez-Muñoz, M. A., Macias Franco, M. R., Narayanasamy, R., and Balagurusamy, N. (2019). Microbially induced calcium carbonate precipitation (MICP) and its potential in bioconcrete: microbiological and molecular concepts. *Front. Mater.* 6, 126. doi:10.3389/fmats.2019.00126

Chang, J.-J., Yeih, W., Hsu, H.-M., and Huang, N.-M. (2009). Performance evaluation of using electrochemical deposition as a repair method for reinforced concrete beams. *Struct. Longev.* 1, 75–93. doi:10.3970/sl.2009.001.075

Chen, Q., Xie, L., Zhu, H., Liu, W., Jiang, Z., Zhang, Z., et al. (2024). Insight into ettringite induced concrete crack healing by electrodeposition: effects of electrochemical parameters and numerical simulations. *Cem. Concr. Compos.* 149, 105504. doi:10.1016/j.cemconcomp.2024.105504

China, M. J. C. A. (2002). Building Press: Beijing, C. Standard for test method of mechanical properties on ordinary concrete.

Chu, H., Liang, Y., Guo, M.-Z., Zhu, Z., Zhao, S., Song, Z., et al. (2020). Effect of electro-deposition on repair of cracks in reinforced concrete. *Constr. Build. Mater.* 238, 117725. doi:10.1016/j.conbuildmat.2019.117725

Ciurli, S., Marzadori, C., Benini, S., Deiana, S., and Gessa, C. (1996). Urease from the soil bacterium Bacillus pasteurii: immobilization on Ca-polygalacturonate. *Soil Biol. Biochem.* 28, 811–817. doi:10.1016/0038-0717(96)00020-x

De Belie, N., and De Muynck, W. (2008). "Crack repair in concrete using biodeposition," in *Concrete repair, rehabilitation and retrofitting II*. Boca Raton, Florida, America: CRC Press, 309–310.

De Muynck, W., Debrouwer, D., De Belie, N., and Verstraete, W. (2008). Bacterial carbonate precipitation improves the durability of cementitious materials. *Cem. Concr. Res.* 38, 1005–1014. doi:10.1016/j.cemconres.2008.03.005

Du, W., Yu, J., He, B., He, Y., He, P., Li, Y., et al. (2020). Preparation and characterization of nano-SiO2/paraffin/PE wax composite shell microcapsules containing TDI for self-healing of cementitious materials. *Constr. Build. Mater.* 231, 117060. doi:10.1016/j.conbuildmat.2019.117060

Emmanuel, A. C., Haldar, P., Maity, S., and Bishnoi, S. (2016). Second pilot production of limestone calcined clay cement in India: the experience. *Indian Concr. J.* 90, 57–63. Available at: https://www.researchgate.net/publication/303435111

Feng, J., Su, Y., and Qian, C. (2019b). Coupled effect of PP fiber, PVA fiber and bacteria on self-healing efficiency of early-age cracks in concrete. *Constr. Build. Mater.* 228, 116810. doi:10.1016/j.conbuildmat.2019.116810

Feng, J., Su, Y., Qian, C. J. C., and Materials, B. (2019a). Coupled effect of PP fiber, PVA fiber and bacteria on self-healing efficiency of early-age cracks in concrete. *concrete* 228, 116810. doi:10.1016/j.conbuildmat.2019.116810

Fode, T. A., Chande Jande, Y. A., and Kivevele, T. (2023). Effects of different supplementary cementitious materials on durability and mechanical properties of cement composite – comprehensive review. *Heliyon* 9, e17924. doi:10.1016/j.heliyon.2023.e17924

Fouladi, A. S., Arulrajah, A., Chu, J., and Horpibulsuk, S. (2023). Application of Microbially Induced Calcite Precipitation (MICP) technology in construction materials: a comprehensive review of waste stream contributions. *Constr. Build. Mater.* 388, 131546. doi:10.1016/j.conbuildmat.2023.131546

Gat, D., Ronen, Z., and Tsesarsky, M. (2017). Long-term sustainability of microbial-induced CaCO3 precipitation in aqueous media. *Chemosphere* 184, 524–531. doi:10.1016/j.chemosphere.2017.06.015

Gebru, K. A., Kidanemariam, T. G., and Gebretinsae, H. K. (2021). Bio-cement production using microbially induced calcite precipitation (MICP) method: a review. *Chem. Eng. Sci.* 238, 116610. doi:10.1016/j.ces.2021.116610

Guan, Y., Li, W., Zhang, Y., Shi, Z., Tan, J., Wang, F., et al. (2017). Aramid nanofibers and poly (vinyl alcohol) nanocomposites for ideal combination of strength and toughness via hydrogen bonding interactions. *Compos. Sci. Technol.* 144, 193–201. doi:10.1016/j.compscitech.2017.03.010

Gujar, P., Santhanam, M., Annabattula, R. K., and Ghosh, P. (2020). Interfacial fracture behaviour between cement paste and epoxy coating-An experimental and phase-field approach. *RILEM Tech. Lett.* 5, 186–193. doi:10.21809/rilemtechlett.2020.133

Guo, L., Xi, B., and Lu, L. (2024b). Strategies to enhance production of metabolites in microbial co-culture systems. *Bioresour. Technol.* 406, 131049. doi:10.1016/j.biortech.2024.131049

Guo, Y., Luo, L., Liu, T., Hao, L., Li, Y., Liu, P., et al. (2024a). A review of low-carbon technologies and projects for the global cement industry. *J. Environ. Sci.* 136, 682–697. doi:10.1016/j.jes.2023.01.021

Homma, D., Mihashi, H., and Nishiwaki, T. J. J. O.A. C. T. (2009). Self-healing capability of fibre reinforced cementitious composites, 7, 217–228.

Hu, L., Li, Z., Kong, L., Wei, J., Chang, J., and Shi, W. (2024). Reassessing the greenhouse effect of biogenic carbon emissions in constructed wetlands. *J. Environ. Manag.* 354, 120263. doi:10.1016/j.jenvman.2024.120263

Int, A.C.-J. A. (2013). Standard test method for measurement of rate of absorption of water by hydraulic-cement concretes, 41, 1–6.

Khaliq, W., and Ehsan, M. B. (2016). Crack healing in concrete using various bio influenced self-healing techniques. *Constr. Build. Mater.* 102, 349–357. doi:10.1016/j.conbuildmat.2015.11.006

Kim, G., Kim, J., and Youn, H. (2018). Effect of temperature, pH, and reaction duration on microbially induced calcite precipitation. *Appl. Sci.* 8, 1277. doi:10.3390/app8081277

Kirkland, C. M., Norton, D., Firth, O., Eldring, J., Cunningham, A. B., Gerlach, R., et al. (2019). Visualizing MICP with X-ray μ-CT to enhance cement defect sealing. *Int. J. Greenh. Gas Control* 86, 93–100. doi:10.1016/j.ijggc.2019.04.019

Krishnan, S., Emmanuel, A. C., and Bishnoi, S. (2019). Hydration and phase assemblage of ternary cements with calcined clay and limestone. *Constr. Build. Mater.* 222, 64–72. doi:10.1016/j.conbuildmat.2019.06.123

Lee, W.-H., Wang, J.-H., Ding, Y.-C., and Cheng, T.-W. (2019). A study on the characteristics and microstructures of GGBS/FA based geopolymer paste and concrete. *Constr. Build. Mater.* 211, 807–813. doi:10.1016/j.conbuildmat.2019.03.291

Leng, G.-Y., Yan, W., Ye, H.-M., Yao, E.-D., Duan, J.-B., Xu, Z.-X., et al. (2024). Evaluation of the injection and plugging ability of a novel epoxy resin in cement cracks. *Petroleum Sci.* 21, 1211–1220. doi:10.1016/j.petsci.2023.10.014

Li, K., and Li, L. (2019). Crack-altered durability properties and performance of structural concretes. *Cem. Concr. Res.* 124, 105811. doi:10.1016/j.cemconres.2019.105811

Li, X., Wanner, A., Hesse, C., Friesen, S., and Dengler, J. (2024). Clinker-free cement based on calcined clay, slag, portlandite, anhydrite, and C-S-H seeding: an SCM-based low-carbon cementitious binder approach. *Constr. Build. Mater.* 442, 137546. doi:10.1016/j.conbuildmat.2024.137546

Liu, F., Pan, B., Zhou, C., and Nie, J. (2024a). Repair interface crack resistance mechanism: a case of magnesium phosphate cement overlay repair cement concrete pavement surface. *Dev. Built Environ.* 17, 100355. doi:10.1016/j.dibe.2024.100355

Liu, H., Zhang, J., Xiao, Y., and He, X. (2024b). Bacterial attachment by crystal in MICP. *Biogeotechnics* 2, 100109. doi:10.1016/j.bgtech.2024.100109

Liu, J., Wang, Z., Xie, G., Li, Z., Fan, X., Zhang, W., et al. (2022). Resource utilization of municipal solid waste incineration fly ash - cement and alkali-activated cementitious materials: a review. *Sci. Total Environ.* 852, 158254. doi:10.1016/j.scitotenv.2022.158254

Lu, C., Li, Z., Wang, J., Zheng, Y., and Cheng, L. (2023). An approach of repairing concrete vertical cracks using microbially induced carbonate precipitation driven by ion diffusion. *Constr. Build. Mater.* 73, 106798. doi:10.1016/j.jobe.2023.106798

Mañosa, J., Calderón, A., Salgado-Pizarro, R., Maldonado-Alameda, A., and Chimenos, J. M. (2024). Research evolution of limestone calcined clay cement (LC3), a promising low-carbon binder – a comprehensive overview. *Heliyon* 10, e25117. doi:10.1016/j.heliyon.2024.e25117

Maruschak, P. O., Konovalenko, I. V., Vuherer, T., Panin, S. V., Berto, F., Danyliuk, I. M., et al. (2016). Analysis and automated fatigue damage evaluation of a 17Mn1Si pipeline steel. *Procedia Struct. Integr.* 2, 1928–1935. doi:10.1016/j.prostr.2016.06.242

Matschei, T., Lothenbach, B., and Glasser, F. P. (2007). The role of calcium carbonate in cement hydration. *Cem. Concr. Res.* 37, 551–558. doi:10.1016/j.cemconres.2006.10.013

Mobley, H., Island, M. D., and Hausinger, R. P. (1995). Molecular biology of microbial ureases. *Microbiol. Rev.* 59, 451–480. doi:10.1128/mmbr.59.3.451-480.1995

Mondal, S., and Ghosh, A. (2023). Biomineralization, bacterial selection and properties of microbial concrete: a review. *J. Build. Eng.* 73, 106695. doi:10.1016/j.jobe.2023.106695

Mutitu, D. K., Wachira, J. M., Mwirichia, R., Thiong'o, J. K., Munyao, O. M., and Muriithi, G. (2019). Influence of Lysinibacillus sphaericus on compressive strength and water sorptivity in microbial cement mortar. *Heliyon* 5, e02881. doi:10.1016/j.heliyon.2019.e02881

Omoregie, A. I., Khoshdelnezamiha, G., Senian, N., Ong, D. E. L., and Nissom, P. M. (2017). Experimental optimisation of various cultural conditions on urease activity for isolated Sporosarcina pasteurii strains and evaluation of their biocement potentials. *Ecol. Eng.* 109, 65–75. doi:10.1016/j.ecoleng.2017.09.012

Pacheco Torgal, F., Miraldo, S., Labrincha, J. A., and De Brito, J. (2012). An overview on concrete carbonation in the context of eco-efficient construction: evaluation, use of SCMs and/or RAC. *Constr. Build. Mater.* 36, 141–150. doi:10.1016/j.conbuildmat.2012.04.066

Panikov, N. S. (2023). "Kinetics of microbial processes: general principles," in *Encyclopedia of soils in the environment*. Second Edition. Academic Press, 168–185.

Pillai, R. G., Gettu, R., Santhanam, M., Rengaraju, S., Dhandapani, Y., Rathnarajan, S., et al. (2019). Service life and life cycle assessment of reinforced concrete systems with limestone calcined clay cement (LC3). *Cem. Concr. Res.* 118, 111–119. doi:10.1016/j.cemconres.2018.11.019

Prajapati, N. K., Agnihotri, A. K., and Basak, N. (2023). Microbial induced calcite precipitation (MICP) a sustainable technique for stabilization of soil: a review. *Mater. Today Proc.* 93, 357–361. doi:10.1016/j.matpr.2023.07.303

Rathivarman, N., Yutharshan, S., Kabishangar, A., Janani, V., Gowthaman, S., Nawarathna, T. H. K., et al. (2024). Evaluating the performance and durability of concrete paving blocks enhanced by bio-cement posttreatment. *Biogeotechnics*, 100103. doi:10.1016/j.bgtech.2024.100103

Scheiner, S. M. (2024). "Greenhouse effect," in *Encyclopedia of biodiversity*. Third Edition. Academic Press, 307–323.

Scott, J. R., and Barnett, T. C. (2006). Surface proteins of gram-positive bacteria and how they get there. *Annu. Rev. Microbiol.* 60, 397–423. doi:10.1146/annurev.micro.60.080805.142256

Scrivener, K., Martirena, F., Bishnoi, S., and Maity, S. (2018). Calcined clay limestone cements (LC3). *Cem. Concr. Res.* 114, 49–56. doi:10.1016/j.cemconres.2017.08.017

Shao, Z., and Cao, M. (2024). Hydration mechanism of limestone calcined clay cement containing calcined coal gangue. *Constr. Build. Mater.* 438, 136906. doi:10.1016/j.conbuildmat.2024.136906

Skibsted, J., and Snellings, R. (2019). Reactivity of supplementary cementitious materials (SCMs) in cement blends. *Cem. Concr. Res.* 124, 105799. doi:10.1016/j.cemconres.2019.105799

Strompinis, N., Sideris, K., Douros, V., Vitsios, I., and Zervos, I. (2014). Self-compacting repair mortars according to BS EN 1504-3. 115, 119. doi:10.1201/b17394-19

Sun, X., Miao, L., Tong, T., and Wang, C. (2019). Study of the effect of temperature on microbially induced carbonate precipitation. *Acta Geotech.* 14, 627–638. doi:10.1007/s11440-018-0758-y

Tiano, P., Biagiotti, L., and Mastromei, G. (1999). Bacterial bio-mediated calcite precipitation for monumental stones conservation: methods of evaluation. *J. Microbiol. methods* 36, 139–145. doi:10.1016/s0167-7012(99)00019-6

Tironi, A., Castellano, C. C., Bonavetti, V. L., Trezza, M. A., Scian, A. N., and Irassar, E. F. (2014). Kaolinitic calcined clays–Portland cement system: hydration and properties. *Constr. Build. Mater.* 64, 215–221. doi:10.1016/j.conbuildmat.2014.04.065

Turner, R., Castro, G. M., Minto, J., El Mountassir, G., and Lunn, R. J. (2023). Treatment of fractured concrete via microbially induced carbonate precipitation: from micro-scale characteristics to macro-scale behaviour. *Constr. Build. Mater.* 384, 131467. doi:10.1016/j.conbuildmat.2023.131467

Wang, X., Huang, Y., Huang, Y., Zhang, J., Fang, C., Yu, K., et al. (2019). Laboratory and field study on the performance of microcapsule-based self-healing concrete in tunnel engineering. *Constr. Build. Mater.* 220, 90–101. doi:10.1016/j.conbuildmat.2019.06.017

Wang, Y., Sun, X., Miao, L., Wang, H., Wu, L., Shi, W., et al. (2023). State-of-the-art review of soil erosion control by MICP and EICP techniques: problems, applications, and prospects. *Sci. Total Environ.* 912, 169016. doi:10.1016/j.scitotenv.2023.169016

Wang, Y., Wang, Z., Ali, A., Su, J., Huang, T., Hou, C., et al. (2024b). Microbial-induced calcium precipitation: bibliometric analysis, reaction mechanisms, mineralization types, and perspectives. *Chemosphere* 362, 142762. doi:10.1016/j.chemosphere.2024.142762

Wang, Y., Yang, M., Shen, F., Zhou, M., and Du, W. (2024a). Conceptual design and life-cycle environmental and economic assessment of low-carbon cement manufacturing processes. *J. Clean. Prod.* 471, 143349. doi:10.1016/j.jclepro.2024.143349

Wang, Z., Su, J., Ali, A., Zhang, R., Yang, W., Xu, L., et al. (2021). Microbially induced calcium precipitation based simultaneous removal of fluoride, nitrate, and calcium by Pseudomonas sp. WZ39: mechanisms and nucleation pathways. *J. Hazard. Mater.* 416, 125914. doi:10.1016/j.jhazmat.2021.125914

Wu, J.-f., Qi, F.-y., Zhang, J., Chen, Z.-w., Wang, H.-l., and Liu, Q.-f. (2024). Modeling of effect of fly ash amount on microstructure and chloride diffusivity of blended fly ash-cement systems. *Constr. Build. Mater.* 443, 137711. doi:10.1016/j.conbuildmat.2024.137711

Yi, H., Zheng, T., Jia, Z., Su, T., and Wang, C. (2021). Study on the influencing factors and mechanism of calcium carbonate precipitation induced by urease bacteria. *J. Cryst. Growth* 564, 126113. doi:10.1016/j.jcrysgro.2021.126113

Zhang, J., Sun, N., Huo, Z., and Chen, J. (2024a). Understanding the synergistic geopolymerization mechanism of multiple solid wastes in ternary geopolymers. *J. Build. Eng.* 95, 110295. doi:10.1016/j.jobe.2024.110295

Zhang, J., Xiao, Y., Cui, H., He, X., and Liu, H. (2024c). Dancing with crystals: bacterial functions and interactions in biomineralization. *Biogeotechnics* 2, 100084. doi:10.1016/j.bgtech.2024.100084

Zhang, W., Shi, F., Duan, X., Kang, W., Feng, C., and Su, F. (2024d). Effect of microbially induced carbonate precipitation (MICP) on the early strength enhancement and micromechanical properties in fly ash blended cement. *Constr. Build. Mater.* 423, 135675. doi:10.1016/j.conbuildmat.2024.135675

Zhang, Y. S., Liu, Y., Sun, X. D., Zeng, W., Xing, H. P., Lin, J. Z., et al. (2024b). Application of microbially induced calcium carbonate precipitation (MICP) technique in concrete crack repair: a review. *Constr. Build. Mater.* 411, 134313. doi:10.1016/j.conbuildmat.2023.134313

Zhao, Y., Wang, T., and Yi, W. (2023). Emergy-accounting-based comparison of carbon emissions of solid waste recycled concrete. *Constr. Build. Mater.* 387, 131674. doi:10.1016/j.conbuildmat.2023.131674

Zunino, F., and Scrivener, K. (2022). Microstructural developments of limestone calcined clay cement (LC3) pastes after long-term (3 years) hydration. *Cem. Concr. Res.* 153, 106693. doi:10.1016/j.cemconres.2021.106693